Analysis of the Spectral Harmonically Enriched Multiscale Coarse Space (SHEM) in 2D*

Martin J. Gander[a], Atle Loneland[b], Talal Rahman[c]

[a]*Section of Mathematics, University of Geneva, Geneva, 1211, Switzerland*
[b]*Norges Bank and Department of Informatics, University of Bergen, Bergen, 5006, Norway*
[c]*Department of Computer science, Electrical engineering and Mathematical sciences, Western Norway University of Applied Sciences, Bergen, 5063, Norway*

Abstract

The Spectral Harmonically Enriched Multiscale (SHEM) coarse space for domain decomposition methods was introduced as a cheaper alternative to GenEO (Generalized Eigenvalue Problems in the Overlap) with similar performance for high contrast problems. In SHEM, one enriches the coarse space with specific, cheaply computable coarse space components to get faster convergence for domain decomposition methods. For high contrast problems, this enrichment leads to robustness against variations and discontinuities in the problem parameters both inside subdomains and across and along subdomain boundaries. We present and analyze here SHEM in 2D based on simple, sparse lower dimensional eigenvalue problems on the interfaces between subdomains, and also a variant that performs equally well in practice, and does not require the solve of eigenvalue problems at all. Our enrichment process naturally reaches the Optimal Harmonically Enriched Multiscale coarse space (OHEM) represented by the full discrete harmonic space. We give a complete convergence analysis of SHEM in 2D, and also test both SHEM variants and OHEM numerically in 2D.

Keywords: Domain Decomposition, Multiscale Coarse Space, SHEM, Harmonic Enrichment.

1. Introduction

It is well known that domain decomposition methods which are based on local communication between subdomains need the addition of a coarse problem in order to be scalable, see for example the books [51, 53] and references therein. The coarse space components of the coarse problem can however do much more than just make a method scalable: work and difficulties of the underlying domain

*This paper should not be reported as representing the views of Norges Bank. The views expressed are those of the authors and do not necessarily reflect those of the Norges Bank.

decomposition method can be transferred into the coarse space, see for example [7] for FETI and [8] for Neumann-Neumann, and an optimal coarse space can even make the underlying domain decomposition method into a direct solver [26, 25, 27], which is then very much related to modern sparse direct solvers like MUMPS, PARDISO and SuperLU [2, 50, 41]. On the other hand, also optimal transmission conditions based on the Dirichlet to Neumann operator can make a Schwarz method into a direct solver, see [45, 21] and references therein. It was indeed the search for such optimal transmission conditions for general decompositions including cross points that led to the idea of the SHEM coarse space: in [28] we discovered transmission conditions which include implicitly an optimal coarse space component that leads to convergence in two iterations, independently of the number of subdomains and underlying equation. These optimal transmission conditions were however difficult and expensive to use in practice, and we found that equivalently we can use a coarse space to the same effect, which is the OHEM space we will see below. For practical purposes, this space is approximated, like the optimal transmission conditions of Dirichlet to Neumann type are approximated. In the case of transmission conditions, this led to the new class of optimized Schwarz methods, which have the same computational cost per iteration as classical Schwarz methods, but converge much faster; for an overview and references, see [21]. Such methods are currently the best iterative solvers for the difficult class of time harmonic wave propagation problems like the Helmholtz equation [33, 34]. In the case of coarse spaces, one can select the most important subspace of the optimal coarse space to increase the performance of the method [26, 7, 8], which is precisely the spirit of SHEM.

This enrichment has become very important for high contrast problems, where classical domain decomposition methods can become very ineffective when the high contrast is not aligned with the decomposition. Domain decomposition methods for problems where the discontinuities in the coefficient are resolved by the coarse mesh and the subdomains have been analyzed thoroughly, (cf. [13, 14, 42, 49, 55, 3] and references therein), and well designed domain decomposition methods can even use coefficient jumps to their advantage and converge faster than without high contrast [23, 32]. In the case where the discontinuous coefficients are not aligned with the coarse mesh or the underlying subdomains, substantial efforts have been made to develop coarse spaces that lead to robust methods with respect to the contrast in the problems. These efforts started with coarse spaces consisting of multiscale finite element basis functions from [39], see [1] for first studies, and [35], where the precise dependence of two level Schwarz methods on the high contrast in a problem was given for the specific case of isolated inclusions, and also the importance of harmonic shape functions was shown for coarse space corrections; see also [6]. A finite volume multiscale coarse space was proposed in [46] and in [47, 48] FETI (finite element tearing and interconnect) methods were analyzed for multiscale problems, see also the earlier important development in [43].

A first idea to enrich the coarse space by eigenfunctions for tackling problems with high contrast can be found in [19, 20], where selected subdomain eigenfunctions are combined with different types of partition of unity functions

$\delta = 2h$	$\delta = 4h$	$\delta = 6h$	$\delta = 8h$	$\delta = 10h$	$\delta = 12h$	$\delta = 14h$	$\delta = 16h$
610(3.6e6)	339(1.1e6)	330(7.1e5)	241(3.5e5)	224(2.9e5)	222(2.5e5)	33(3.4e1)	30(2.8e1)

Table 1: Iteration and condition number estimate for the distribution in Figure 1 for a classical two level additive Schwarz preconditioner when increasing the overlap δ, with $h = \frac{1}{128}$, $H = 16h$ and contrast $\alpha = 10^6$.

and the importance of the initial coarse space based on multiscale and energy minimizing basis functions is discussed, see also [15], and [31] for a detailed comparison of this approach with the more recent techniques below. A different way to construct a coarse space using eigenfunctions of the Dirichlet to Neumann map of each subdomain was proposed in [11]. This approach was later improved by solving a generalized eigenvalue problem in the overlaps [52], leading to the very successful GenEO (generalized eigenproblems in the overlap) coarse space. This started substantial research for such enriched coarse spaces, like the SHEM coarse space [29, 4, 44, 17, 18], the ACMS (approximate component mode synthesis) coarse space [36], and the AGDSW (adaptive generalized Dryja–Smith–Widlund) coarse space [37, 38]; for a recent historical review on these developments, and also a detailed comparison that shows that all these approaches are very much related, see [24].

We present here for SHEM in 2D a simple procedure that allows us to systematically enrich a given coarse space, up to a maximum degree where it becomes a direct solver. A natural extension of SHEM to 3D can be found in [17]. Since our interest is in high contrast problems, we start with a classical multiscale finite element coarse space. The multiscale finite element method was developed to cope with problems that have many spatial scales [39], and was developed not with coarse spaces for domain decomposition methods in mind. The idea is to replace the classical finite element shape functions by harmonic functions, i.e. functions that solve the underlying equation locally. An important problem in multiscale finite element methods is what boundary conditions one should impose on these harmonic shape functions. The approach we propose here for SHEM can also be used to enrich a multiscale finite element space, and if combined with non-overlapping subdomain solves, will in the limit reach the fine scale finite element solution, which is an important property of our enrichment process.

We start with a numerical experiment to motivate our harmonic enrichment process. The problem configuration is shown in Figure 1. We show in Table 1 the iteration numbers and condition number estimates for a two level additive Schwarz preconditioner when increasing the overlap, where the coarse space is the multiscale coarse space introduced in [35]. We see that initially increasing the overlap improves the method, but increasing further does not help much, until we reach the overlap $\delta = 14h$, where a substantial improvement happens. Why is this so? Looking at Figure 1, we see that there are many highly conductive channels across the interfaces, which end however then within

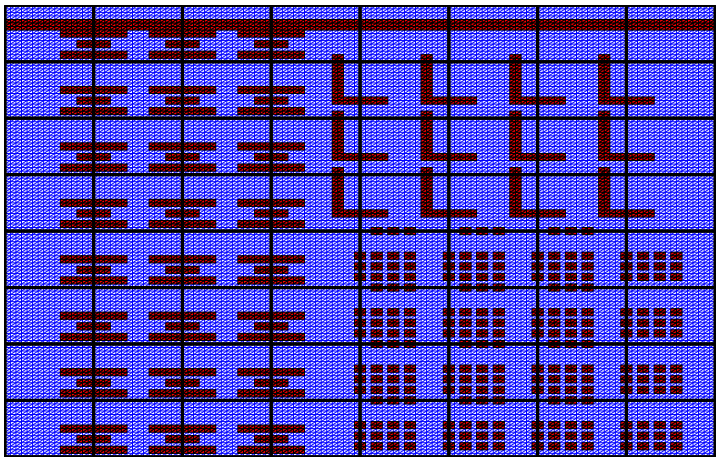

Figure 1: Distribution of α for a geometry with $h = \frac{1}{128}$, $H = 16h$. The regions marked with red are where α has a large value.

the subdomains[1], which means that an error component will travel with very little damping across the overlap through these channels. Following the original maximum principle argument of Schwarz, the error will thus not diminish substantially, until the overlap includes the entire channel, at which point rapid convergence will set in, see [27, Section 4] for more details. This is a typical case where the underlying domain decomposition method has difficulties if the overlap is too small, and these difficulties can be transferred into the coarse space. The present multiscale coarse space is however not good enough to handle these difficulties.

The idea of SHEM first introduced in [30] almost a decade ago is to systematically transfer such difficulties into the coarse space by enriching it with well chosen harmonic functions. In contrast to GenEO, where the enrichment process is motivated by a generalized eigenvalue problem that appears in the abstract condition number estimate, in SHEM the enrichment functions are chosen based on the domain decomposition iteration itself, which for Schwarz methods has only very recently been fully understood [10], long after the first introduction of SHEM in [30]. We study for SHEM this enrichment based on an eigenvalue problem on the interfaces between the subdomains, which leads to the name Spectral Harmonically Enriched Multiscale coarse space. For SHEM, we solve lower dimensional sparse eigenvalue problems in the construction phase,

[1]Channels going across entire subdomains like the long channel at the top do not pose problems for convergence, since the classical Schwarz convergence mechanism based on the maximum principle then still works.

which is much cheaper than the construction based on volume subdomain eigenvalue problems in GenEO, or Dirichlet to Neumann eigenvalue problems and the Schur complement based constructions in AGDSW. We then also show that one can obtain a good harmonic enrichment without solving eigenvalue problems at all, which we call the Non-Spectral alternative for the Harmonically Enriched Multiscale coarse space (NSHEM). For the given numerical examples, NSHEM works equally well.

2. Preliminaries

2.1. The Model Problem

We consider as our model problem the elliptic boundary value problem

$$\begin{aligned} -\nabla \cdot (\alpha(x)\nabla u) &= f \qquad \text{in } \Omega, \\ u &= 0 \qquad \text{on } \partial\Omega, \end{aligned} \tag{1}$$

where Ω is a polygonal domain in $\mathbb{R}^2$, $f \in L^2(\Omega)$ and $\alpha \in L^\infty(\Omega)$ with the property that $\alpha \geq \alpha_0$ for some positive constant α_0.

The weak formulation of (1) is: find $u \in H_0^1(\Omega)$ such that

$$a(u,v) := \int_\Omega \alpha(x)\nabla u \cdot \nabla v \, dx = \int_\Omega fv \, dx \quad \forall v \in H_0^1(\Omega). \tag{2}$$

We discretize (2) with standard P_1 finite elements on a mesh $\mathcal{T}_h$ of Ω such that $\overline{\Omega} = \bigcup_{K\in\mathcal{T}_h} K$, where the finite element space is defined as $V_h^0(\Omega) := \{v \in C_0(\Omega) : v|_K \in P_1(K)\}$. The discrete problem corresponding to (2) is: find $u_h \in V_h^0(\Omega)$ such that

$$a(u_h, v) = \int_\Omega fv \, dx \quad \forall v \in V_h^0(\Omega). \tag{3}$$

Without loss of generality we will assume that the coefficient α is piecewise constant over each element K, i.e., $\alpha(x) = \alpha_K$ for all $x \in K$.

We also introduce the following notation: for positive constants c and C independent of the mesh parameters h, H, the overlap δ (which we will define below) and the coefficient α, we define $u \simeq v$, $x \succeq y$ and $w \preceq z$ as $cu \leq v \leq Cu$, $x \geq cy$ and $w \leq Cz$ respectively. Here, u, v, x, y, w and z denote norms of some functions.

2.2. Subdomains

Let Ω be partitioned into non-overlapping open, connected polygonal substructures $\{\Omega_i : i = 1, \ldots, N\}$ such that $\overline{\Omega} = \bigcup_{i=1}^N \overline{\Omega}_i$, where each $\overline{\Omega}_i$ is assumed to consist of elements from $\mathcal{T}_h(\Omega)$. By extending each subdomain Ω_i with a distance δ' in each direction, we create a further decomposition of Ω into overlapping subdomains $\{\Omega_i'\}_{i=1}^N$. This corresponds to a geometric overlap of $\delta = 2\delta'$, where δ is the width of the overlap. We consider here only the specific case of small overlap $\delta = 2h$, but a slight modification of the proof will also cover the

case of minimal geometric overlap h. We denote the layer of elements in Ω_i touching the boundary $\partial\Omega_i$ by Ω_i^h and assume that the triangles corresponding to this layer are shape regular and define the minimum diameter of these triangles as $h_i := \min_{K\in\mathcal{T}_h(\Omega_i^h)} h_K$, where h_K is the diameter of the triangle K. We define the interface between two subdomains to be the open edge shared by the subdomains, i.e., $\overline{\Gamma}_{ij} := \overline{\Omega}_i \cap \overline{\Omega}_j$. The sets of vertices of elements in $\mathcal{T}_h(\Omega)$ (nodal points) belonging to Ω, Ω_i, $\partial\Omega$, $\partial\Omega_i$ and Γ_{ij} are denoted by Ω_h, Ω_{ih}, $\partial\Omega_h$, $\partial\Omega_{ih}$ and Γ_{ijh}. With each interface we define the space of finite element functions restricted to Γ_{ij} and zero on $\partial\Gamma_{ij}$ as $V_h^0(\Gamma_{ij})$.

The weighted L^2-inner product and the corresponding weighted L^2-norm is defined as $(u,v)_{L^2_\alpha(G)} := (\alpha(x)u,v)_{L^2(G)}$ and $\|u\|^2_{L^2_\alpha(G)} := (u,u)_{L^2_\alpha(G)}$, where G is some domain contained in Ω.

We define the restriction of the bilinear form $a(\cdot,\cdot)$ to an interface, $\Gamma_{ij}\subset\Gamma$, shared by two subdomains as

$$a_{\Gamma_{ij}}(u,v) := \left(\alpha_{|\Gamma_{ij}}(x)D_{x^t}u, D_{x^t}v\right)_{L^2(\Gamma_{ij})},$$

where $\alpha_{|\Gamma_{ij}}(x) := \lim_{y\in\Omega_i\to x}\alpha(y)$ and D_{x^t} denotes the tangent derivative with respect to Γ_{ij}. Since α may have discontinuities across Γ_{ij} the corresponding restrictions of the bilinear forms $a_{\Gamma_{ij}}(\cdot,\cdot)$ and $a_{\Gamma_{ji}}(\cdot,\cdot)$ to Γ_{ij} for the subdomains Ω_i and Ω_j sharing Γ_{ij} will differ. In order to obtain continuous coarse basis functions across subdomain interfaces, we therefore need to choose a common bilinear form for each interface shared by two subdomains when constructing the coarse basis functions in Section 3. One choice is to define the following bilinear form on each interface Γ_{ij},

$$\bar{a}_{\Gamma_{ij}}(u,v) := (\overline{\alpha}_{ij}(x)D_{x^t}u, D_{x^t}v)_{L^2(\Gamma_{ij})},$$

where $\overline{\alpha}_{ij}$ is taken as the maximum of $\alpha_{|\Gamma_{ij}}$ and $\alpha_{|\Gamma_{ji}}$. An evident, but important relation following directly from this definition is that

$$\bar{a}_{\Gamma_{ij}}(u,v) \simeq a_{\Gamma_{ij}}(u,v) + a_{\Gamma_{ji}}(u,v). \tag{4}$$

The geometric domain decomposition induces a decomposition of $V_h^0(\Omega)$ into local subspaces: for each Ω_i', the corresponding local subspace is

$$V_i := \left\{v\in V_h^0(\Omega) \,:\, \mathrm{supp}(v)\subset\Omega_i'\right\}.$$

This yields a decomposition of $V_h^0(\Omega)$,

$$V_h^0(\Omega) = V_0 + \sum_{i=1}^N V_i,$$

where the coarse space, V_0, is a special space which we will define later. For $i=0,\ldots,N$ we define the projection like operators $T_i\colon V_h^0(\Omega)\to V_i$ as

$$a(T_iu,v) := a(u,v) \qquad \forall v\in V_i, \tag{5}$$

and introduce the operator

$$T := T_0 + T_1 + \cdots + T_N. \tag{6}$$

This allows us to replace the original problem (3) by the equation

$$Tu = g, \tag{7}$$

where $g = \sum_{i=0}^{N} g_i$ and $g_i = T_i u$. Note that g_i can be computed without knowing the solution u of (3).

2.3. Eigenvalue Problems on Interfaces

The first harmonic enrichment in SHEM is based on solutions of local eigenvalue problems along the interfaces between subdomains:

Definition 2.1 (Generalized Eigenvalue Problem)**.** *For each interface $\Gamma_{ij} \subset \Gamma$, we define the generalized eigenvalue problem: Find ψ and λ, such that*

$$\bar{a}_{\Gamma_{ij}}(\psi, v) = \lambda b_{\Gamma_{ij}}(\psi, v) \qquad \forall v \in V_h^0(\Gamma_{ij}), \tag{8}$$

where $b_{\Gamma_{ij}}(\psi, v) := h_i^{-1} \sum_{k \in \Gamma_{ijh}} \beta_k \psi_k v_k$ and $\beta_k = \sum_{\substack{K \in \mathcal{T}_h(\Omega) \\ k \in \mathrm{dof}(K)}} \alpha_K$.

The following lemma is a slight modification of Lemma 2.11 in [52] and provides important estimates for the eigenfunction projection.

Lemma 2.2. *Define $M := \dim(V_h^0(\Gamma_{ij}))$ and let the eigenpairs $\{(\psi_{\Gamma_{ij}}^k, \lambda_{ij}^k)\}_{k=1}^{\dim(V_h^0(\Gamma_{ij}))}$ of the generalized eigenvalue problem (8) be ordered such that*

$$0 < \lambda_{ij}^1 \leq \lambda_{ij}^2 \ldots \leq \lambda_{ij}^M \quad \text{and} \quad b_{\Gamma_{ij}}(\psi_{\Gamma_{ij}}^k, \psi_{\Gamma_{ij}}^l) = \delta_{kl} \quad \text{for any} \quad 1 \leq k, l \leq M.$$

Then, the projection for any integer $0 \leq m_{ij} \leq M$

$$\Pi_{\mathrm{m}} v := \sum_{k=1}^{m_{ij}} b_{\Gamma_{ij}}(v, \psi_{\Gamma_{ij}}^k) \psi_{\Gamma_{ij}}^k$$

is a-orthogonal, and therefore

$$|\Pi_{\mathrm{m}} v|_{\bar{a}_{\Gamma_{ij}}} \leq |v|_{\bar{a}_{\Gamma_{ij}}} \quad \text{and} \quad |v - \Pi_{\mathrm{m}} v|_{\bar{a}_{\Gamma_{ij}}} \leq |v|_{\bar{a}_{\Gamma_{ij}}}, \qquad \forall v \in V_h^0(\Gamma_{ij}). \tag{9}$$

In addition we also have the approximation estimate

$$\|v - \Pi_{\mathrm{m}} v\|_{b_{\Gamma_{ij}}}^2 \leq \frac{1}{\lambda_{ij}^{m_{ij}+1}} |v - \Pi_{\mathrm{m}} v|_{\bar{a}_{\Gamma_{ij}}}^2, \qquad \forall v \in V_h^0(\Gamma_{ij}). \tag{10}$$

Proof. Following the lines of the proof given in [52, Lemma 2.11], we start out by recognizing that since both $\bar{a}_{\Gamma_{ij}}$ and $b_{\Gamma_{ij}}$ are positive definite, we may reduce the

generalized eigenvalue problem to a standard eigenvalue problem, where standard spectral theory guarantees the existence of eigenpairs $\{(\psi^k_{\Gamma_{ij}}, \lambda^k_{ij})\}_{k=1}^{\dim(V_h^0(\Gamma_{ij}))}$, for which the eigenvalues $\{\lambda^k_{ij}\}_{k=1}^{\dim(V_h^0(\Gamma_{ij}))}$ are positive. In addition, we may choose the eigenvectors such that they form a basis of $V_h^0(\Gamma_{ij})$ and satisfy the orthogonality conditions

$$\bar{a}_{\Gamma_{ij}}(\psi^k_{\Gamma_{ij}}, \psi^l_{\Gamma_{ij}}) = b_{\Gamma_{ij}}(\psi^k_{\Gamma_{ij}}, \psi^l_{\Gamma_{ij}}) = 0 \quad \forall k \neq l, \quad |\psi^k_{\Gamma_{ij}}|^2_{\bar{a}_{\Gamma_{ij}}} = \lambda^k_{ij} \text{ and } \|\psi^k_{\Gamma_{ij}}\|^2_{b_{\Gamma_{ij}}} = 1.$$

Now, any $v \in V_h^0(\Gamma_{ij}))$ may be expressed as

$$v = \sum_{k=1}^{\dim(V_h^0(\Gamma_{ij}))} b_{\Gamma_{ij}}(v, \psi^k_{\Gamma_{ij}})\psi^k_{\Gamma_{ij}}.$$

The $\bar{a}_{\Gamma_{ij}}$-orthogonality states that

$$\left|\sum b_{\Gamma_{ij}}(v, \psi^k_{\Gamma_{ij}})\psi^k_{\Gamma_{ij}}\right|^2_{\bar{a}_{\Gamma_{ij}}} = \sum b_{\Gamma_{ij}}(v, \psi^k_{\Gamma_{ij}})^2 \left|\psi^k_{\Gamma_{ij}}\right|^2_{\bar{a}_{\Gamma_{ij}}}.$$

From this we have

$$|v|^2_{\bar{a}_{\Gamma_{ij}}} = |\Pi_{\mathrm{m}} v|^2_{\bar{a}_{\Gamma_{ij}}} + |v - \Pi_{\mathrm{m}} v|^2_{\bar{a}_{\Gamma_{ij}}},$$

and (9) follows directly. To prove (10), we start by using the $b_{\Gamma_{ij}}$ - orthonormality of the eigenfunctions

$$\begin{aligned}
\|v - \Pi_{\mathrm{m}} v\|^2_{b_{\Gamma_{ij}}} &= \left\| \sum_{k=m_{ij}+1}^{\dim(V_h^0(\Gamma_{ij}))} b_{\Gamma_{ij}}(v, \psi^k_{\Gamma_{ij}})\psi^k_{\Gamma_{ij}} \right\|^2_{b_{\Gamma_{ij}}} \\
&= \sum_{k=m_{ij}+1}^{\dim(V_h^0(\Gamma_{ij}))} b_{\Gamma_{ij}}(v, \psi^k_{\Gamma_{ij}})^2 \frac{1}{\lambda^k_{ij}} |\psi^k_{\Gamma_{ij}}|^2_{\bar{a}_{\Gamma_{ij}}} \\
&\leq \frac{1}{\lambda^{m_{ij}+1}_{ij}} \sum_{k=m_{ij}+1}^{\dim(V_h^0(\Gamma_{ij}))} b_{\Gamma_{ij}}(v, \psi^k_{\Gamma_{ij}})^2 |\psi^k_{\Gamma_{ij}}|^2_{\bar{a}_{\Gamma_{ij}}} \\
&= \frac{1}{\lambda^{m_{ij}+1}_{ij}} |v - \Pi_{\mathrm{m}} v|^2_{\bar{a}_{\Gamma_{ij}}}.
\end{aligned}$$

In the last steps we used the fact that $|\psi^k_{\Gamma_{ij}}|^2_{\bar{a}_{\Gamma_{ij}}} = \lambda^k_{ij}$, that the eigenvalues are ordered in increasing order and that the eigenfunctions are $\bar{a}_{\Gamma_{ij}}$-orthogonal. □

3. Construction of the Coarse Space

In this section we define the coarse space for SHEM. It is a multiscale finite element space enriched with harmonic functions based on the generalized eigenvalue problem (8) defined on each interface shared by two subdomains. In order to explain the construction in detail, we start by introducing discrete harmonic functions before we describe how SHEM is constructed.

3.1. Discrete Harmonic Functions

For each non-overlapping subdomain Ω_i we define the restriction of V_h to $\bar{\Omega}_i$ as

$$V_h(\Omega_i) := \left\{ v_{|\bar{\Omega}_i} : v \in V_h \right\},$$

and the corresponding subspace with zero Dirichlet boundary conditions as

$$V_h^0(\Omega_i) := \{ v \in V_h(\Omega_i) : v(x) = 0 \quad \text{for} \quad x \in \partial\Omega_{ih} \}.$$

Clearly $V_h^0(\Omega_i) \subset V_h(\Omega_i)$. Now let $\mathcal{P}_i : V_h(\Omega_i) \to V_h^0(\Omega_i)$ be the a-orthogonal projection of a function $u \in V_h(\Omega_i)$ onto $V_h^0(\Omega_i)$ such that

$$a_i(\mathcal{P}_i u, v) = a_i(u, v) \qquad \forall v \in V_h^0(\Omega_i), \tag{11}$$

where $a_i(\cdot,\cdot)$ is the restriction of $a(\cdot,\cdot)$ to Ω_i and define $\mathcal{H}_i u := u - \mathcal{P}_i u$ as the discrete harmonic counterpart of u, i.e.

$$\begin{aligned} a_i(\mathcal{H}_i u, v) &= 0 \qquad \forall v \in V_h^0(\Omega_i), & (12)\\ \mathcal{H}_i u(x) &= u(x) \qquad x \in \partial\Omega_{ih}. & (13) \end{aligned}$$

A function $u \in V_h(\Omega_i)$ is locally discrete harmonic if $\mathcal{H}_i u = u$. If all restrictions to subdomains of a function $u \in V_h$ are locally discrete harmonics, i.e.,

$$u_{|\Omega_i} = \mathcal{H}_i u_{|\Omega_i} \qquad \text{for } i = 1, \ldots, N,$$

then we say u is a discrete harmonic function. For any function $u \in V_h$, this gives a decomposition of u into discrete harmonic parts and local projections, i.e. $u = \mathcal{H}u + \mathcal{P}u$.

With the operator $\mathcal{H}$, we can introduce the space of discrete harmonic functions as

$$\tilde{V}_h = \mathcal{H}V_h = \{ u \in V_h : \forall i = 1, \ldots, N,\ u_{|\Omega_i} = \mathcal{H}_i u_{|\Omega_i} \}.$$

For a two level method that considers a non-overlapping partitioning of Ω as subdomains, this space is the optimal coarse space, in the sense that the domain decomposition methods becomes a direct solver. We will in the following sections show how one can approximate this space in a systematic manner by carefully including into the coarse space the most important components of $\tilde{V}_h$ not already included in our initial multiscale finite element coarse space. In the limit, these enrichment strategies will reach the Optimal Harmonically Enriched Multiscale (OHEM) coarse space $\tilde{V}_h$, and allow us to turn the method into a direct solver. This is an important property of SHEM, and such Schur type complement structures are also used in modern multifrontal direct solvers like MUMPS [2], which was developed with domain decomposition methods in a joint project [5], see also PARDISO [50] and SuperLU [41].

With this in mind, we are now ready to define the coarse basis functions.

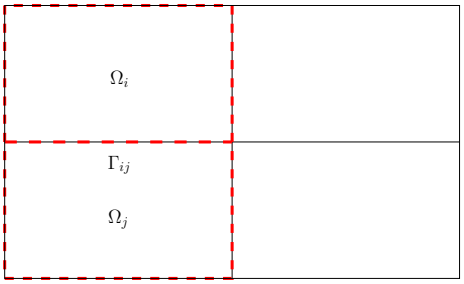

Figure 2: Support of a spectral basis function $p^k_{\Gamma_{ij}}$ corresponding to the interface Γ_{ij}.

3.2. Multiscale Basis Functions

Following [39], the multiscale finite element coarse space, which we will consider as our initial coarse space for SHEM, consists of vertex based discrete harmonic functions associated with each vertex of the polygon Ω_i. More formally, for each vertex x^k of the subdomain Ω_i that does not belong to $\partial\Omega$ and for each internal edge $\Gamma_{ij} \subset \Omega_i$ that touches x^k, we solve the 1D boundary value problem

$$\begin{aligned} \bar{a}_{\Gamma_{ij}}(\hat{\phi}^{ms}_{ik}, v) &= 0 \quad \forall v \in V_h^0(\Gamma_{ij}), \qquad \text{(interface values)} \\ \hat{\phi}^{ms}_{ik}(x^k) &= 1 \quad \text{at the vertex } x^k \text{ of } \Omega_i, \\ \hat{\phi}^{ms}_{ik} &= 0 \quad \text{at the other vertex.} \end{aligned}$$

Then the solution is extended inside Ω_i to form ϕ^{ms}_{ik} using the values of $\hat{\phi}^{ms}_{ik}$ as boundary conditions on the edges touching x^k and zero on the remaining edges

$$\begin{aligned} a_i(\phi^{ms}_{ik}, v) &= 0 \quad \forall v \in V_h^0(\Omega_i), \qquad \text{(harmonic extension inside)} \\ \phi^{ms}_{ik}(x) &= \hat{\phi}^{ms}_{ik} \quad x \in \Gamma_{ij}, \quad x^k \in \partial\Gamma_{ij}. \\ \phi^{ms}_{ik}(x) &= 0 \quad x \in \partial\Omega_i \setminus \Gamma_{ij}, \quad x^k \in \partial\Gamma_{ij}. \end{aligned} \tag{14}$$

The solutions corresponding to each k are then glued together in a natural manner to form multiscale hat functions and extended with zero to the rest of Ω.

3.3. Spectral Basis Functions

Let $\psi^k_{\Gamma_{ij}}$ be the k-th eigenfunction of the generalized eigenvalue problem (8) on each interface Γ_{ij}. We then define the spectral basis functions associated with the interface Γ_{ij} as the discrete harmonic extension of each of the eigenfunctions $\psi^k_{\Gamma_{ij}}$

$$\begin{aligned} a_l(p^k_{\Gamma_{ij}}, v) &= 0 \quad \forall v \in V_h^0(\Omega_l) \text{ and } l \in \{i, j\}, \\ p^k_{\Gamma_{ij}} &= \psi^k_{\Gamma_{ij}} \quad x \in \Gamma_{ij}, \\ p^k_{\Gamma_{ij}} &= 0 \quad x \in (\partial\Omega_i \cup \partial\Omega_j) \setminus \Gamma_{ij}. \end{aligned} \tag{15}$$

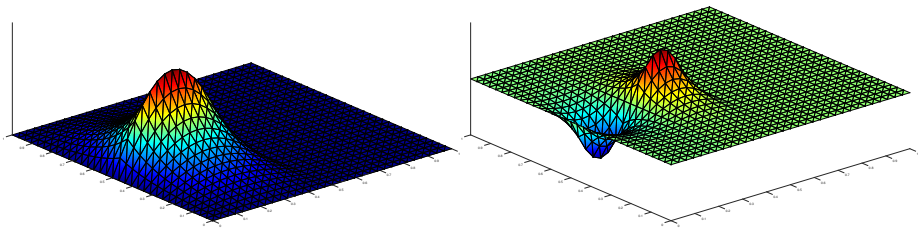

Figure 3: Plot of the spectral basis functions for $h = 1/32$ and $H = 16h$. *Left:* first order spectral basis functions. *Right:* second order spectral basis functions.

Each solution is then extended with zero to the rest of Ω in order to make the functions global. Note that the support of the function is still local. See Figure 2 for an illustration of Ω_i, Ω_j and Γ_{ij}.

SHEM is then defined as the span of these two sets of basis functions,

$$V_0 := \operatorname{span}\{\{\phi_k^{ms}\}_{k=1}^{n_\nu} \cup \{\{p_{\Gamma_{ij}}^l\}_{l=1}^{m_{ij}}\}_{\Gamma_{ij}\subset\Gamma}\}, \tag{16}$$

where n_ν is the number of interior subdomain vertices of Ω.

An example of the first and second order spectral basis function, i.e., the basis functions corresponding the smallest and second smallest eigenvalue on Γ_{ij}, is given in Figure 3 for a problem with $\alpha = 1$ and mesh parameters $H = 1/2$ and $h = 1/32$.

4. Analysis of the Preconditioner

In this section we define a suitable interpolation operator into the SHEM coarse space V_0 and provide the necessary bounds for the operator in order to apply the classical abstract Schwarz framework. The aforementioned interpolation operator is a composition of the standard multiscale interpolation operator and a new interpolation operator for the spectral basis functions.

The multiscale interpolation operator is defined as

$$I_{\text{ms}}u := \sum_{k=1}^{n_\nu} u(x^k)\phi_k^{\text{ms}}, \tag{17}$$

where n_ν is the number of internal vertices, i.e. vertices of the polygon Ω_i which are not on $\partial\Omega$. The spectral interpolation operator is defined as

$$\Pi_{\text{m}}u := \sum_{\Gamma_{ij}\subset\Gamma}\sum_{k=1}^{m_{ij}} b_{\Gamma_{ij}}(u, p_{\Gamma_{ij}}^k)p_{\Gamma_{ij}}^k. \tag{18}$$

Combining these two, the new coarse space interpolation operator $I_0\colon V_h^0(\Omega) \to V_0$ is defined as

$$I_0u := I_{\text{ms}}u + \Pi_{\text{m}}\left(u - I_{\text{ms}}u\right). \tag{19}$$

Lemma 4.1 (Stable Decomposition)**.** *For all $u \in V_h$ and $u_i \in V_i(\Omega), i = 1, \ldots, N$, there exists a representation $u = \sum_{i=0}^{N} u_i$ such that*

$$a(u_0, u_0) + \sum_{i=1}^{N} a(u_i, u_i) \preceq C_0^2 a(u, u), \tag{20}$$

where $u_0 = I_0 u$, $C_0^2 \simeq \left(1 + \frac{1}{\lambda_{m+1}}\right)$ and $\lambda_{m+1} := \min_i \min_{\Gamma_{ij} \subset \partial\Omega_i} \lambda_{m_{ij}+1}^{ij}$.

Proof. Let $w := u - u_0$ and define $u_i := I_h(\theta_i w)$, where I_h is the nodal piecewise linear continuous interpolation operator on the fine mesh $\mathcal{T}_h(\Omega)$ and θ_i is a partition of unity function with respect to the partition $\{\Omega_i'\}_{i=1}^N$. θ_i is zero on $\Omega \setminus \Omega_i'$ and $\theta_i(x) = 1$ for $x \in \Omega_{ih}$, $\theta_i(x) = 1/2$ for $x \in \Gamma_{ijh}$, and $\theta_i(x) = 1/N_c$ when $x = x^k$. N_c is here defined as the number of overlapping subdomains that contain k as an internal degree of freedom.

We start by estimating $a(u_0, u_0) = \sum_{i=1}^{N} a_i(u_0, u_0)$. From the energy minimizing property of discrete harmonic functions we have for all $v \in V_h(\Omega_i)$ where $v = u_0$ on the boundary of $\partial\Omega_i$ and $v = u$ on Ω_{ih} that

$$\begin{aligned} a_i(u_0, u_0) &\leq a_i(v, v) = a_i(v - u + u, v - u + u) \\ &\leq 2a_i(v - u, v - u) + 2a_i(u, u). \end{aligned}$$

Using the fact that $u - v$ is zero on Ω_{ih} and at the domain decomposition vertices, we then get

$$a_i(v - u, v - u) \preceq \sum_{\Gamma_{ij} \subset \partial\Omega_i} h_i \|u - u_0\|_{b_{\Gamma_{ij}}}^2. \tag{21}$$

By applying Lemma 2.2 we have for each edge $\Gamma_{ij} \subset \partial\Omega_i$ that

$$\begin{aligned} \|u - u_0\|_{b_{\Gamma_{ij}}}^2 &= \|(u - I_{\mathrm{ms}} u) - \Pi_{\mathrm{m}}(u - I_{\mathrm{ms}} u)\|_{b_{\Gamma_{ij}}}^2 \\ &\preceq \frac{1}{\lambda_{ij}^{m_{ij}+1}} |(u - I_{\mathrm{ms}} u) - \Pi_{\mathrm{m}}(u - I_{\mathrm{ms}} u)|_{\bar{a}_{\Gamma_{ij}}}^2 \\ &\preceq \frac{1}{\lambda_{ij}^{m_{ij}+1}} |u - I_{\mathrm{ms}} u|_{\bar{a}_{\Gamma_{ij}}}^2 \preceq \frac{1}{\lambda_{ij}^{m_{ij}+1}} |u|_{\bar{a}_{\Gamma_{ij}}}^2. \end{aligned} \tag{22}$$

The last inequality follows straightforwardly from Lemma 2.2 and the $\bar{a}_{\Gamma_{ij}}$-stability property of the 1D multiscale operator that follows from its energy-minimality w.r.t. $|\cdot|_{\bar{a}_{\Gamma_{ij}}}$. By defining $\lambda_{m_i+1}^i := \min_{\Gamma_{ij} \subset \partial\Omega_i} \lambda_{m_{ij}+1}^{ij}$ and using (4) we

have that

$$\begin{aligned}\sum_{\Gamma_{ij}\subset\partial\Omega_i}\frac{h_i}{\lambda_{ij}^{m_{ij}+1}}|u|^2_{\bar{a}_{\Gamma_{ij}}} &\simeq \sum_{\Gamma_{ij}\subset\partial\Omega_i}\frac{h_i}{\lambda_{ij}^{m_{ij}+1}}\left(|u|^2_{a_{\Gamma_{ij}}}+|u|^2_{a_{\Gamma_{ji}}}\right)\\ &\preceq \frac{1}{\lambda^i_{m_i+1}}\left(|u|^2_{a,\Omega_i^h}+\sum_{\Gamma_{ij}\subset\partial\Omega_i}|u|^2_{a,\Omega_j^h}\right)\\ &\leq \frac{1}{\lambda^i_{m_i+1}}\left(|u|^2_{a,\Omega_i}+\sum_{\Gamma_{ij}\subset\partial\Omega_i}|u|^2_{a,\Omega_j}\right), \qquad (23)\end{aligned}$$

where in the second inequality above we extend the estimate from the boundary to the subdomain layer (see e.g. [12, Equation (4.16) and Remark 4.2]), while in the last inequality we extend from the subdomain layer to the whole of the subdomain. Then, by summing over each subdomain and defining $\lambda_{m+1} := \min_i \lambda^i_{m_i+1}$ completes the first part of the proof. The two seminorms $|\cdot|_{a,\Omega_i}$ and $|\cdot|_{a,\Omega_i^h}$ above are the restriction of $|\cdot|_a$ to Ω_i and Ω_i^h.

Now we need to provide the same type of bound for the local terms u_i, i.e.

$$\sum_{i=1}^N a(u_i,u_i) \preceq \frac{1}{\lambda_{m+1}}a(u,u). \qquad (24)$$

Since we are only considering the case of two layers of overlap ($\delta = 2h$) and by adding and subtracting $u-u_0$ we have

$$\begin{aligned}a(u_i,u_i) &= a_{\Omega_i'\setminus\overline{\Omega}_i}(u_i,u_i)+a_{\Omega_i}(u_i-(u-u_0)+(u-u_0),u_i-(u-u_0)+(u-u_0))\\ &\leq a_{\Omega_i'\setminus\overline{\Omega}_i}(u_i,u_i)+2a_{\Omega_i}(u-u_0,u-u_0)+2a_{\Omega_i}(u_i-(u-u_0),u_i-(u-u_0))\\ &\simeq a_{\Omega_i}(u-u_0,u-u_0)+\sum_{\Gamma_{ij}\subset\partial\Omega_i}h_i\|u-u_0\|^2_{b_{\Gamma_{ij}}}.\end{aligned}$$

The last term in the inequality above has already been estimated so finally we have that

$$\sum_{i=0}^N a(u_i,u_i) \preceq \left(1+\frac{1}{\lambda_{m+1}}\right)a(u,u), \qquad (25)$$

which completes the proof of (20).

□

Remark 4.2. The theoretical results developed in this section easily extend to the case of minimal overlap h. The only modifications needed in the proof of Lemma 4.1 are for the local components $a(u_i,u_i)$. Instead of splitting the overlapping subdomain Ω_i' into $\Omega_i'\setminus\overline{\Omega}_i$ and Ω_i, one instead splits the overlapping zone of Ω_i', i.e., the part that is shared by two or more subdomains, into the part outside of the coarse grid elements and the part that is inside the coarse grid elements and then proceed in a similar fashion as in the proof above.

Remark 4.3. With more restrictions on the geometric distribution of α we are able to improve this estimate, but for arbitrary α that can vary rapidly on the fine scale $\sim h$ we are only able to extend with a distance h from the boundary of the subdomains into the subdomain layer. See for example Remark 4.2 in [12] for more details.

Theorem 4.4. *The condition number of the two level Schwarz operator (6) with the SHEM coarse space (16) can be bounded by*

$$\kappa(\mathbf{TA}) \preceq \omega C_0^2(\rho(\mathcal{E}_{ij}) + 1), \tag{26}$$

where C_0 is defined as in Lemma 4.1, $\omega = 1$, $\mathbf{TA}$ is the matrix representation of our preconditioned system and $\rho(\mathcal{E})$ is the spectral radius of $\mathcal{E}$ defined in Assumption 2 below.

Proof. Following the Schwarz framework, cf. [53, 51], we need to prove three assumptions:

Assumption (1)**.** *This assumption is the stable decomposition which we have already proved in Lemma 4.1.*

Assumption (2)**.** *Let $0 \leq \mathcal{E}_{ij} \leq 1$ be the minimal values that satisfy*

$$a(u_i, u_j) \leq \mathcal{E}_{ij} a(u_i, u_i)^{1/2} a(u_j, u_j)^{1/2}, \qquad \forall u_i \in V_i,\ \forall u_j \in V_j\ i, j = 1, \ldots, N$$

Define $\rho(\mathcal{E})$ to be the spectral radius of $\mathcal{E} = \{\mathcal{E}_{ij}\}$.

Assumption (3)**.** *Let $\omega > 0$ be the minimal constant such that*

$$a(u_i, u_i) \leq \omega \tilde{a}_i(u_i, u_i), \qquad u_i \in V_i.$$

We use exact bilinear forms, i.e., $\tilde{a}_i(u_i, u_i) = a(u_i, u_i)$, so in our case $\omega = 1$ for $i = 0, \ldots, N$. □

5. Non-Spectral alternative for Harmonic Enrichment

Similar coarse basis functions as the ones constructed in the previous section may also be constructed without solving eigenvalue problems on the interfaces. Instead we may solve local lower dimensional problems and extend the solutions harmonically inside each subdomain in the same manner as for the eigenfunctions.

For this variant of SHEM we construct the basis functions by solving on each interface Γ_{ij} the 1D problem[2]

$$\begin{aligned} \bar{a}_{\Gamma_{ij}}(\phi^k_{\Gamma_{ij}}, v) &= b_{\Gamma_{ij}}(g^k, v) \qquad \forall v \in V_h^0(\Gamma_{ij}), \\ \phi^k_{\Gamma_{ij}} &= 0 \qquad x \in \partial\Gamma_{ij}, \end{aligned} \tag{27}$$

[2]This can be intuitively understood as a first step in a power iteration in order to compute an eigendecomposition, and we try to excite the corresponding mode.

where $b_{\Gamma_{ij}}(\cdot,\cdot)$ is given in Definition 2.1 and the alternating function g^k is defined in the following way: let $\gamma_{ij} : [0,1] \to \Gamma_{ij}$ be a parametrization of the interface Γ_{ij}, where $\gamma_{ij}(0)$ and $\gamma_{ij}(1)$ describe the end points of Γ_{ij} and let k denote the number of the basis functions used for enrichment. The alternating function $g^k(x)$ is then defined for each k by

$$g^k(\gamma_{ij}(t)) := \begin{cases} 1, & t \in [0, \frac{1}{k}], \\ -1, & t \in (\frac{1}{k}, \frac{2}{k}], \\ \vdots & \\ (-1)^{k-1}, & t \in (\frac{k-1}{k}, 1]. \end{cases}$$

Other choices for g^k are also possible: one could for instance choose g^k to be a family of sine functions like $g^k = \sin k\pi x$ for an interface of length 1, or hierarchical basis functions starting with the hat function spanning the entire interval, followed by two hat functions spanning half the interval and so on, see Subsection 6.1 for more details. In any case the crucial part for achieving the same robust behavior as in the eigenfunction case is that we use the weighted L^2 inner product on the right hand side in (27).

Next, we extend these solutions harmonically inside the two subdomains sharing Γ_{ij} as an edge in the same manner as for the eigenfunctions, i.e. for each subdomain sharing Γ_{ij}, we solve

$$\begin{aligned} a_i(\chi^k_{\Gamma_{ij}}, v) &= 0 \qquad \forall v \in V_h^0(\Omega_i), \\ \chi^k_{\Gamma_{ij}} &= \phi^k_{\Gamma_{ij}} \quad x \in \Gamma_{ij}, \\ \chi^k_{\Gamma_{ij}} &= 0 \qquad x \in (\partial\Omega_i \cup \partial\Omega_j) \setminus \Gamma_{ij}, \end{aligned} \tag{28}$$

and extend the solution with zero to the rest of Ω.

The Non-Spectral alternative for the Harmonically Enriched Multiscale (NSHEM) coarse space is then defined as the span of the two sets of basis functions

$$V_0^* := \text{span}\{\{\phi_k^{ms}\}_{k=1}^{n_\nu} \cup \{\{\chi^l_{\Gamma_{ij}}\}_{l=1}^{m_{ij}}\}_{\Gamma_{ij}\subset\Gamma}. \tag{29}$$

We will also refer to the above basis functions as non-spectral functions. An example of such functions for $k = 1$ and $k = 2$ are given in Figure 4 for a problem with $\alpha = 1$ and mesh parameters $H = 1/2$ and $h = 1/32$. We see a close resemblance to the spectral basis functions given in Figure 3; for a more quantitative comparison, we computed the Rayleigh quotient and obtained for the first order non-spectral basis function v_1 the value $\frac{v_1 A v_1^T}{v_1 v_1^T} = 0.0783$, and for the second order non-spectral basis function $\frac{v_2 A v_2^T}{v_2 v_2^T} = 0.2468$. This is indeed very close to the values obtained for the eigenfunction basis variant shown in Figure 3, for which we obtained $\frac{v_1 A v_1^T}{v_1 v_1^T} = 0.0780$ and $\frac{v_2 A v_2^T}{v_2 v_2^T} = 0.2937$. In the next section, we show with numerical examples that the performance for these non-spectral, much cheaper variants of the coarse enrichment is almost identical to the behavior of the eigenfunction variant.

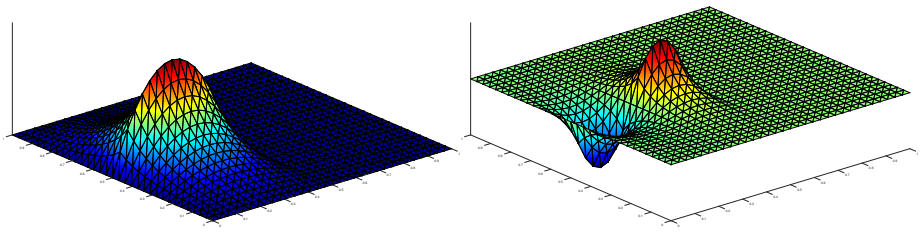

Figure 4: Plot of the non-spectral basis functions for $h = 1/32$ and $H = 16h$. *Left:* first order non-spectral basis functions. *Right:* second order non-spectral basis functions.

6. Numerical Results

We now present extensive numerical experiments for the SHEM and NSHEM coarse spaces solving problem (1) on a unit square domain, i.e. $\Omega = (0,1)^2$, where the right hand side is chosen to be $f = 1$, and the coefficient $\alpha(x)$ represents various (possibly discontinuous) distributions. We test the new coarse spaces with the two level additive Schwarz preconditioner and conjugate gradients, where the coarse spaces have been enriched with different numbers of spectral and non-spectral basis functions on each interface. For all numerical examples, we run the preconditioned conjugate gradient method until the l_2 norm of the initial residual is reduced by a factor of 10^6, that is, until $\|r_i\|_2/\|r_0\|_2 \leq 10^{-6}$. The coefficient $\alpha(x)$ for all the numerical examples is equal to 1, except in the areas marked with red where the value of $\alpha(x)$ is equal to $\hat{\alpha}$.

6.1. Comparison of SHEM and NSHEM

We start by showing that SHEM and the three variants of NSHEM introduced in the previous sections have similar performance. To do so, we use the distribution of α with three inclusions of different size crossing interfaces between subdomains in Figure 5. We test the case where the multiscale coarse space is enriched with three basis functions on each interface (SHEM_3) and compare the number of iterations and condition number in Table 2 to NSHEM_3^a, which denotes the variant with three piecewise constant alternating function g^k in the definition (27), NSHEM_3^s, which uses a family of sine functions, i.e.,

$$g^k(\gamma_{ij}(t)) := \sqrt{\frac{2h}{H}} \sin\left(\frac{k\pi h t}{H}\right) \qquad t \in [0,1].$$

For NSHEM_3^h, which uses hierarchical basis functions, g^k is defined as

$$g^k(\gamma_{ij}(t)) := \begin{cases} 1 - 2^r \left| t - t_{mp_k} \right|, & t \in [s, s + \frac{1}{2^{r-1}}], \\ 0, & \text{elsewhere}, \end{cases}$$

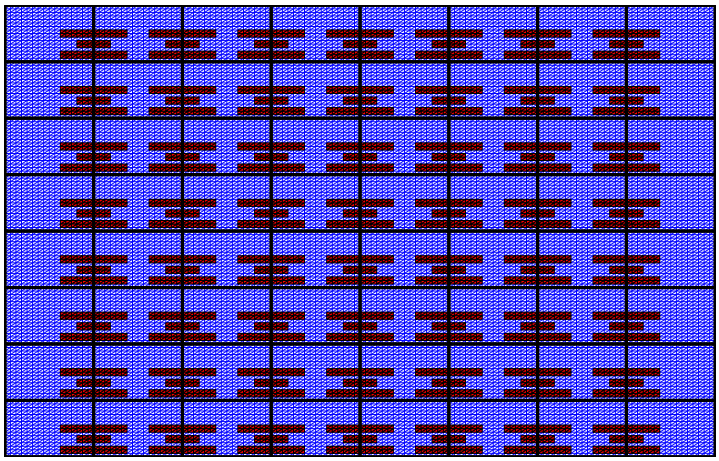

Figure 5: Distribution of α for a geometry with $h = \frac{1}{128}$, $H = 16h$. The regions marked with red are where α has a large value.

Type:	SHEM_3	NSHEM_3^a	NSHEM_3^s	NSHEM_3^h
$\hat{\alpha}$	#it. (κ)	#it. (κ)	#it. (κ)	#it. (κ)
10^0	13 (5.19e0)	13 (5.50e0)	13 (5.19e0)	17 (8.26e0)
10^2	18 (7.42e0)	19 (7.74e0)	19 (7.80e0)	20 (7.58e0)
10^4	19 (7.44e0)	19 (7.49e0)	19 (7.44e0)	20 (7.60e0)
10^6	19 (7.44e0)	19 (7.49e0)	19 (7.44e0)	21 (7.61e0)

Table 2: Comparison of the iteration count and condition number estimate for SHEM_3 and the three NSHEM_3 variants for the distribution given in Figure 5 with $h = \frac{1}{128}$, $H = 16h$.

where $r = \lfloor \lg k \rfloor + 1$ is the refinement level the hierarchical basis function k corresponds to, t_{mp_k} is the midpoint of the interval $[s, s + \frac{1}{2^{r-1}}]$ and $s = \frac{k}{2^{r-1}} - 1$ is the location parameter of the corresponding basis function on the hierarchical refinement level. The parametrization of Γ_{ij} is the same as in the definition of the alternating functions case.

We see from the results in Table 2 that the performance of the four variants is very similar. In fact, for the first three variants of the coarse enrichment, the performance of the method is basically identical.

We next revisit the distribution of α given in Figure 1, and compare SHEM_i and NSHEM_i^a with a varying number of basis functions $i = 1, 2, 3, 4$ on each interface. We state the number of iterations and condition number for each run in the Table 3 and 4. We see again that the performance of SHEM_i and NSHEM_i^a is very similar, and the solver becomes robust for the same number $i = 3$ of enrichment functions, corresponding to the number of inclusions across the interfaces.

	MS	SHEM_1	SHEM_2	SHEM_3	SHEM_4
dim.	49	161	273	385	497
$\hat{\alpha}$	#it. (κ)	#it. (κ)	#it. (κ)	#it. (κ)	#it. (κ)
10^0	21 (1.29e1)	16 (7.45e0)	15 (5.99e0)	13 (5.19e0)	13 (5.15e0)
10^2	122 (3.74e2)	70 (1.17e2)	47 (6.70e1)	19 (6.77e0)	16 (5.66e0)
10^4	367 (3.64e4)	248 (1.10e4)	187 (6.22e3)	19 (6.78e0)	17 (5.73e0)
10^6	610 (3.64e6)	423 (1.10e6)	290 (6.22e5)	19 (6.78e0)	17 (5.73e0)

Table 3: Iteration count and condition number estimate for the distribution in Figure 1 for the classical multiscale coarse space (MS) and different numbers of spectral basis functions $i = 1, 2, 3, 4$ in SHEM_i with $h = \frac{1}{128}$, $H = 16h$.

	NSHEM_1^a	NSHEM_2^a	NSHEM_3^a	NSHEM_4^a
dim.	161	273	385	497
$\hat{\alpha}$	#it. (κ)	#it. (κ)	#it. (κ)	#it. (κ)
10^0	16 (7.52e0)	14 (6.06e0)	13 (5.50e0)	13 (5.23e0)
10^2	71 (1.17e2)	49 (6.92e1)	19 (6.79e0)	17 (5.74e0)
10^4	256 (1.11e4)	130 (6.45e3)	20 (6.81e0)	20 (6.67e0)
10^6	454 (1.11e6)	221 (6.45e5)	20 (6.81e0)	20 (6.67e0)

Table 4: Iteration count and condition number estimate for the distribution in Figure 1 for different numbers of non-spectral basis functions $i = 1, 2, 3, 4$ in NSHEM_i^a with $h = \frac{1}{128}$, $H = 16h$.

6.2. An Adaptive Variant of SHEM

In Table 5 on the left we give the number of iterations and condition number for an adaptive version we call $\text{SHEM}_{\text{adapt}}$ in the case of the distribution of α given in Figure 1: on each interface shared by two subdomains we enrich the coarse space with spectral basis functions corresponding to eigenvalues below a certain threshold. By comparing the eigenvalues to the eigenvalues of the Laplacian we may choose the threshold in such a way that we only include spectral functions corresponding to eigenvalues that are smaller than the smallest eigenvalue of the Laplacian on each interface. Eigenvalues below this threshold will correspond to discontinuities along the subdomain boundaries; this is illus-

$\text{SHEM}_{\text{adapt}}$		
$\hat{\alpha}$	#it. (κ)	dim.
10^0	21 (1.29e1)	49
10^2	25 (1.10e1)	233
10^4	25 (1.09e1)	233
10^6	25 (1.09e1)	233

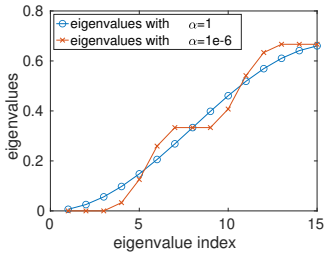

Table 5: Left: iteration and condition number estimate for the distribution in Figure 1 for $\text{SHEM}_{\text{adapt}}$ with $h = \frac{1}{128}$, $H = 16h$. Right: example eigenvalue distribution for an interface with three channels to illustrate how to determine the threshold for robustness with respect to high contrast. With $\alpha = 1$, the three smallest eigenvalues are $6.4049e-03$, $2.5373e-02$ and $5.6177e-02$, whereas with large contrast $\alpha = 1e6$ the three smallest eigenvalues are $2.2698e-08$, $1.3394e-07$ and $2.7194e-07$.

OHEM	non-overlapping	overlapping
$\hat{\alpha}$	#it. (κ)	#it. (κ)
10^0	1 (1)	10 (5)
10^2	1 (1)	13 (5)
10^4	1 (1)	13 (5)
10^6	1 (1)	13 (5)

Table 6: Iteration and condition number estimate for OHEM applied to the distribution in Figure 1 with $h = \frac{1}{128}$, $H = 16h$.

trated in the plot on the right in Table 5 for an example interface with three channels, and we see that indeed three eigenvalues are smaller with the high contrast parameter $\alpha = 1e-6$ than the smallest eigenvalue for the Laplacian case, i.e. $\alpha = 1$; see also [27] for more details related to different geometries of high contrast channels and their relation to the eigenvalue distribution.

By studying the dimension of the enriched coarse space in Table 5 we see that by a proper choice of the cut-off criteria the method is completely insensitive to any discontinuity inside subdomains and along subdomain boundaries. Also, if we count the number of high conducting regions in Figure 1 crossing the interfaces, we see that the number of eigenfunctions needed on each interface equals the number of inclusions or channels crossing it.

6.3. An Example of OHEM

If all of the spectral basis functions corresponding to each interface are included, then the coarse space spans the full discrete harmonic function space $\tilde{V}_h$, which is the Optimal Harmonically Enriched Multiscale (OHEM) coarse space, and the method can be made into a direct solver: The subdomain solves are only used to incorporate the influence of the right hand side function into the solution, while the full harmonic space then connects and shifts them correctly, and overlap is not needed any more. OHEM then represents in some sense a direct factorization based on Schur complements which are also used very effectively in modern multifrontal direct solvers like MUMPS [2], PARDISO [50] and SuperLU [41]. In Table 6, we show some numerical results for the non-overlapping case, where we obtain the solution in one iteration, and the corresponding overlapping method, where we see that the error the additive Schwarz preconditioner commits in the overlap to remain symmetric (see [16, 22] for more details) prevents the method from converging in one iteration. This can be easily fixed using Restricted Additive Schwarz instead which treats the overlap correctly, as shown in [29], see also [26]. OHEM is not really a practical method, since the coarse space is very big, but it is of great theoretical interest, since it defines precisely which object a robust coarse space should approximate, and this is how we discovered SHEM and NSHEM, see also [10] where this optimal coarse space is discovered differently with a spectral analysis of the Schwarz iteration operator, and [28] where the complete coarse space information is encoded in transmission conditions between subdomains.

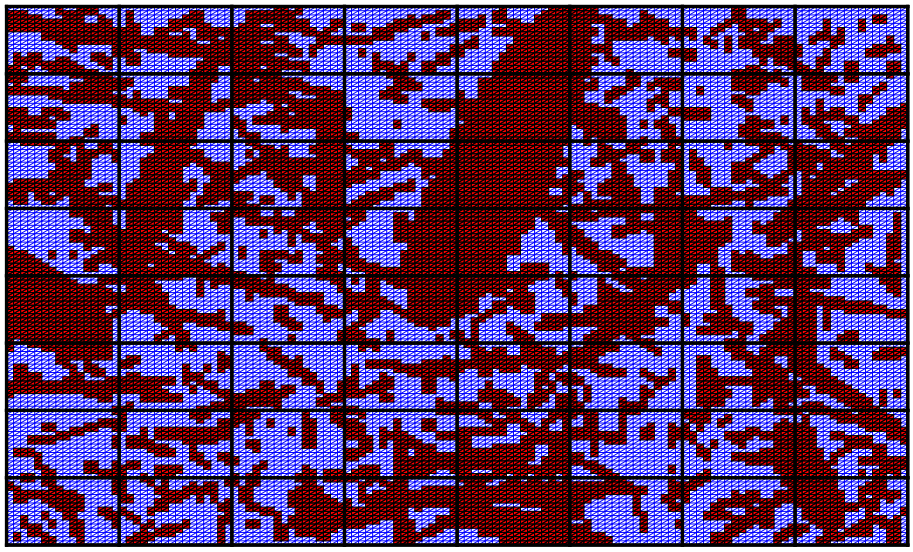

Figure 6: Distribution of α for a geometry with $h = \frac{1}{128}$, $H = 16h$. The regions marked with red are where α has a large value.

Type:	SHEM_3		$\text{SHEM}_{\text{adapt}}$	
$\hat{\alpha}$	#it. (κ)	dim.	#it. (κ)	dim.
10^0	13 (5.19e0)	385	16 (7.45e0)	161
10^2	22 (9.47e0)	385	25 (1.07e1)	239
10^4	23 (9.60e0)	385	26 (1.11e1)	236
10^6	24 (9.59e0)	385	28 (1.08e1)	236

Table 7: Iteration and condition number estimate for the distribution in Figure 6 comparing SHEM_3 and $\text{SHEM}_{\text{adapt}}$ with $h = \frac{1}{128}$, $H = 16h$.

6.4. Highly Irregular Conductivities and Subdomains

We now test the case where we allow the distribution of α to be highly irregular. Inspired by an example in [54] we consider a slightly modified version of it, as shown in Figure 6. For this case we choose the threshold for the adaptive variant $\text{SHEM}_{\text{adapt}}$ in such a way that we are guaranteed at least one spectral basis function on each edge. The number of iterations and condition numbers for increasing $\hat{\alpha}$ are given in Table 7 for SHEM_3 and $\text{SHEM}_{\text{adapt}}$. We see from the table that the dimension of the coarse space is still lower than the dimension for the local subspaces. In addition, we see that the performance of $\text{SHEM}_{\text{adapt}}$ with a substantially smaller coarse space is still comparable to SHEM_3 with three enrichment functions on each interface.

In order to test SHEM on more realistic problems, we consider now the case where Ω is subdivided into irregular fine triangles for the fine mesh and irregular subdomains arising from the graph partitioning software METIS [40] for the subdomains and the coarse mesh. For the first two experiments, we consider only the adaptive variant $\text{SHEM}_{\text{adapt}}$ and compare it with the standard multiscale

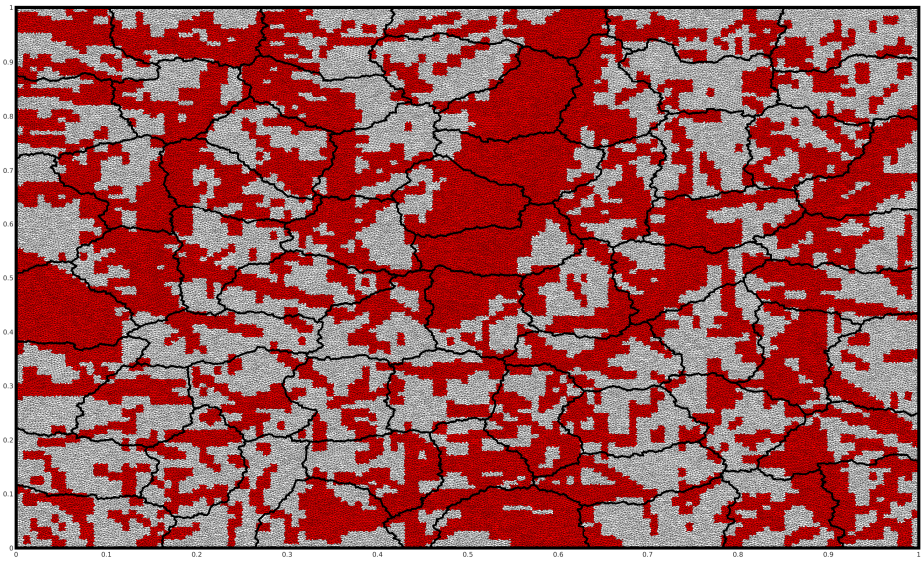

Figure 7: Distribution of α for a geometry discretized with 226918 irregular triangles and partitioned into 64 irregular subdomains with METIS. The regions marked with red are where α has a large value. The largest subdomain has 1889 dofs.

coarse space without enrichment denoted by MS. For our first example, we modify the distribution given in Figure 6 by discretizing it with an irregular mesh such that the largest diameter of the elements is $1/256$. We then partition the mesh into irregular subdomains using METIS, see Figure 7. The tolerance for including spectral functions into the coarse space is set to $\tau = 1/32$ and the iteration count and condition number estimate for `pcg` are given in Table 8 where we also report the size of the coarse space. For the second example, we consider the same fine grid and coarse grid as in the previous example, but now the coefficients α are taken as the permeability field from the bottom layer of the SPE 10th comparative solution project [9], see Figure 8. We compare the results of MS with $\text{SHEM}_{\text{adapt}}$ for three different choices of the tolerance τ and

Type:	MS		$\text{SHEM}_{\text{adapt}}$	
$\hat{\alpha}$	#it. (κ)	dim.	#it. (κ)	dim.
10^0	47 (3.55e1)	101	21 (6.95e0)	676
10^2	143 (7.49e2)	101	28 (1.11e1)	738
10^4	699 (3.50e4)	101	28 (1.10e1)	738
10^6	898 (3.41e6)*	101	30 (1.10e1)	738

* Stagnation.

Table 8: Comparison of the iteration count and condition number estimate for MS (without enrichment) and $\text{SHEM}_{\text{adapt}}$ with tolerance $\tau = 1/32$ for the problem given in Figure 7. The number of coarse dofs for both methods is given in the columns next to the iteration count and condition number estimate. Stagnation is here defined as two consecutive iterations of `pcg` to be equal.

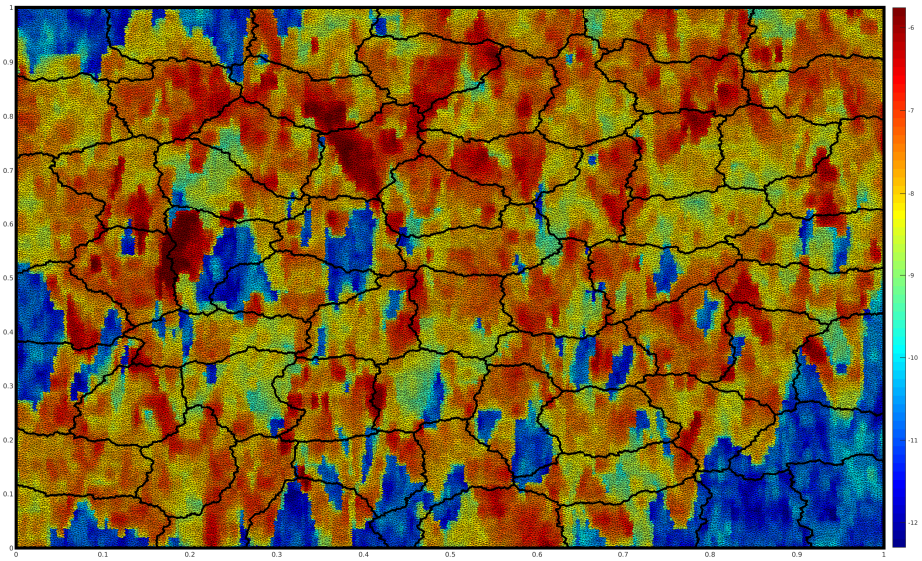

Figure 8: Base 10 logarithm of the permeability field going from -6 (red) to -12 (blue) corresponding to the SPE10 Bottom Layer test case for a geometry discretized with 226918 irregular triangles and partitioned into 64 irregular subdomains with METIS. The largest subdomain has 1889 dofs.

Type:	MS		$\text{SHEM}_{\text{adapt}}$	
τ	#it. (κ)	dim.	#it. (κ)	dim.
$\frac{1}{64}$	124 (3.75e2)	101	30 (1.23e1)	489
$\frac{1}{32}$	124 (3.75e2)	101	27 (1.09e1)	646
$\frac{1}{16}$	124 (3.75e2)	101	23 (7.72e0)	910

Table 9: Comparison of the iteration count and condition number estimate for MS (without enrichment) and $\text{SHEM}_{\text{adapt}}$ for the problem given in Figure 8. The number of coarse dofs for both methods is given in the columns next to the iteration count and condition number estimate. τ is defined as the tolerance for the inclusion of eigenfunctions with eigenvalue smaller than τ.

report the iteration count and condition number estimate for `pcg` in Table 8 in addition to the number of coarse basis functions for each choice of τ. For our third and last example we compare the performance of SHEM_i with NSHEM_i^s, NSHEM_i^h and NSHEM_i^a in order to show that the non-spectral variants perform at the same level as the spectral variant also for harder problems where the discretization and subdomain decomposition are irregular. For this purpose, we consider the same problem as in the first example, see Figure 7, and compare the performance of the coarse spaces for $i = 1, \ldots, 8$. We report the iteration count and condition number estimate for `pcg` along with the dimension of the coarse space in Table 10. We observe that all NSHEM-methods perform almost as well as SHEM. Also, after enough basis function are added to the coarse space, there is no gain in enriching the coarse space further.

These examples show that $\text{SHEM}_{\text{adapt}}$ performs very well even for very hard

	SHEM_i	NSHEM_i^s	NSHEM_i^h	NSHEM_i^a	
i	#it. (κ)	#it. (κ)	#it. (κ)	#it. (κ)	dim.
1	920(2.33e6)	961(2.19e6)	980(2.34e6)	997(1.95e6)	258
2	229(8.31e4)	278(2.78e5)	354(4.11e5)	346(3.82e5)	418
3	140(7.01e4)	139(6.93e4)	144(7.29e4)	164(6.52e4)	577
4	45(3.29e1)	70(7.86e2)	137(7.54e4)	104(7.26e3)	733
5	42(3.35e1)	43(3.33e1)	115(5.38e4)	54(7.76e2)	888
6	37(1.79e1)	41(1.93e1)	54(2.09e3)	50(7.73e2)	1040
7	34(1.79e1)	39(1.78e1)	38(1.79e1)	41(1.75e1)	1191
8	34(1.79e1)	38(1.79e1)	37(1.79e1)	40(1.76e1)	1338

Table 10: Comparison of the iteration count and condition number estimate for SHEM_i, NSHEM_i^s, NSHEM_i^h and NSHEM_i^a for the problem given in Figure 7 with $i = 1 \dots 8$ and $\alpha = 10^6$.

problems and much better than MS that only uses the initial multiscale coarse space. For all choices of the tolerance τ, the $\text{SHEM}_{\text{adapt}}$ is insensitive to the irregularities of both the subdomain/coarse partitioning and the fine grid and also with respect to the high contrast in the underlying material coefficient, without the dimension of the coarse space becoming larger than the dimension of the largest subdomain and thus the coarse solve never becomes the bottleneck of the method for the given examples. In specific situations, like in all domain decomposition methods, e.g. when the number of subdomains becomes extremely large, then the coarse space problem needed could become larger than the largest subdomain problem, and then multilevel variants could become necessary, a topic which deserves further study.

7. Conclusion

We presented two spectral enrichment techniques for SHEM (adaptive and non-adaptive) and a detailed condition number estimate for an associated two level additive Schwarz preconditioner in 2D that shows that the method becomes robust in the context of high contrast problems. Our first enrichment process uses lower dimensional eigenvalue problems on interfaces between subdomains and extends these solutions harmonically inside each of the corresponding subdomains sharing the interface. The second is even cheaper, not based on eigenvalue problems, using only solutions of lower dimensional variants of the original problem on the interfaces between subdomains. We showed numerically that the performance of both is comparable, and also when completing the enrichment to the full discrete harmonic space, SHEM becomes optimal (OHEM) and the method turns into a direct solver, very much related to modern multifrontal solvers like MUMPS, PARDISO and SuperLU. This property shows that SHEM coarse spaces are not just useful for high contrast elliptic model problems for which we analyzed SHEM in this manuscript. The concept of SHEM and OHEM is a fundamental tool to structurally tackle many other partial differential equations, even if there is no analysis so far. SHEM will always lead in fine to rapid convergence, since it is based on the approximation of an optimal coarse space which contains all coarse space components necessary to turn the domain

decomposition method into a direct solver, and gives guidelines on which coarse functions to keep, and this independently of the PDE one is solving. For more information on how to choose coarse functions, see [10], where the functions to choose are related to slowly converging components of the Schwarz iteration operator, with a construction on how to identify them locally.

Acknowledgment

We thank Professor Leszek Marcinkowski for his comments, particularly for pointing out to us that Definition 2.1 in our earlier version did not cover the case where elements with large coefficients would touch subdomain boundaries at only one point. This work was supported by the Swiss National Science Foundation.

References

[1] J. Aarnes and T. Y. Hou. Multiscale domain decomposition methods for elliptic problems with high aspect ratios. *Acta Math. Appl. Sin. Engl. Ser.*, 18(1):63–76, 2002.

[2] P. R. Amestoy, I. S. Duff, J.-Y. L'Excellent, and J. Koster. MUMPS: a general purpose distributed memory sparse solver. In *International Workshop on Applied Parallel Computing*, pages 121–130. Springer, 2000.

[3] P. E. Bjørstad, M. Dryja, and E. Vainikko. Additive Schwarz methods without subdomain overlap and with new coarse spaces. In *Domain Decomposition Methods in Sciences and Engineering (Beijing, 1995)*, pages 141–157. Wiley, Chichester, 1997.

[4] P. E. Bjørstad, M. J. Gander, A. Loneland, and T. Rahman. Does SHEM for Additive Schwarz work better than predicted by its condition number estimate? In *Domain Decomposition Methods in Science and Engineering XXIV 24*, pages 129–137. Springer, 2018.

[5] P. E. Bjørstad, J. Koster, and P. Krzyżanowski. Domain decomposition solvers for large scale industrial finite element problems. In *Applied Parallel Computing. New Paradigms for HPC in Industry and Academia: 5th International Workshop, PARA 2000 Bergen, Norway, June 18–20, 2000 Proceedings 5*, pages 373–383. Springer, 2001.

[6] M. Buck, O. Iliev, and H. Andrä. Domain decomposition preconditioners for multiscale problems in linear elasticity. *Numerical Linear Algebra with Applications*, 25(5):e2171, 2018.

[7] F. Chaouqui, M. J. Gander, and K. Santugini-Repiquet. Optimal coarse spaces for FETI and their approximation. In *Numerical Mathematics and Advanced Applications ENUMATH 2017*, pages 931–939. Springer, 2019.

[8] F. Chaouqui, M. J. Gander, and K. Santugini-Repiquet. A continuous analysis of Neumann–Neumann methods: Scalability and new coarse spaces. *SIAM Journal on Scientific Computing*, 42(6):A3785–A3811, 2020.

[9] M. Christie, M. Blunt, et al. Tenth SPE comparative solution project: A comparison of upscaling techniques. In *SPE Reservoir Simulation Symposium*. Society of Petroleum Engineers, 2001.

[10] F. Cuvelier, M. J. Gander, and L. Halpern. Fundamental coarse space components for Schwarz methods with crosspoints. In *Domain Decomposition Methods in Science and Engineering XXVI*, pages 41–52. Springer, 2023.

[11] V. Dolean, F. Nataf, R. Scheichl, and N. Spillane. Analysis of a two-level Schwarz method with coarse spaces based on local Dirichlet-to-Neumann maps. *Comput. Methods Appl. Math.*, 12(4):391–414, 2012.

[12] M. Dryja and M. Sarkis. Additive average Schwarz methods for discretization of elliptic problems with highly discontinuous coefficients. *Computational Methods in Applied Mathematics*, 10(2):164–176, 2010.

[13] M. Dryja, M. V. Sarkis, and O. B. Widlund. Multilevel Schwarz methods for elliptic problems with discontinuous coefficients in three dimensions. *Numer. Math.*, 72(3):313–348, 1996.

[14] M. Dryja, B. F. Smith, and O. B. Widlund. Schwarz analysis of iterative substructuring algorithms for elliptic problems in three dimensions. *SIAM J. Numer. Anal.*, 31(6):1662–1694, 1994.

[15] Y. Efendiev, J. Galvis, R. Lazarov, and J. Willems. Robust domain decomposition preconditioners for abstract symmetric positive definite bilinear forms. *ESAIM Math. Model. Numer. Anal.*, 46(5):1175–1199, 2012.

[16] E. Efstathiou and M. J. Gander. Why restricted additive Schwarz converges faster than additive Schwarz. *BIT*, 43(suppl.):945–959, 2003.

[17] E. Eikeland, L. Marcinkowski, and T. Rahman. Overlapping Schwarz methods with adaptive coarse spaces for multiscale problems in 3D. *Numerische Mathematik*, 142(1):103–128, 2019.

[18] E. Eikeland, L. Marcinkowski, and T. Rahman. An adaptively enriched coarse space for Schwarz preconditioners for p_1 discontinuous Galerkin multiscale finite element problems. *IMA Journal of Numerical Analysis*, 41(4):2873–2895, 2021.

[19] J. Galvis and Y. Efendiev. Domain decomposition preconditioners for multiscale flows in high-contrast media. *Multiscale Model. Simul.*, 8(4):1461–1483, 2010.

[20] J. Galvis and Y. Efendiev. Domain decomposition preconditioners for multiscale flows in high contrast media: reduced dimension coarse spaces. *Multiscale Model. Simul.*, 8(5):1621–1644, 2010.

[21] M. J. Gander. Optimized Schwarz methods. *SIAM J. Numer. Anal.*, 44(2):699–731, 2006.

[22] M. J. Gander. Schwarz methods over the course of time. *Electron. Trans. Numer. Anal.*, 31:228–255, 2008.

[23] M. J. Gander and O. Dubois. Optimized Schwarz methods for a diffusion problem with discontinuous coefficient. *Numerical Algorithms*, 69(1):109–144, 2015.

[24] M. J. Gander and L. Halpern. Piece-wise constant, linear and oscillatory: a historical introduction to spectral coarse spaces with focus on Schwarz methods. In *Domain Decomposition Methods in Science and Engineering XXVII*, pages 189–198. Springer, 2023.

[25] M. J. Gander, L. Halpern, and K. Santugini. Discontinuous coarse spaces for DD-methods with discontinuous iterates. In *Domain Decomposition Methods in Science and Engineering XXI. Springer LNCSE*. Springer, 2014.

[26] M. J. Gander, L. Halpern, and K. Santugini. A new coarse grid correction for RAS/AS. In *Domain Decomposition Methods in Science and Engineering XXI. Springer LNCSE*. Springer, 2014.

[27] M. J. Gander, L. Halpern, and K. Santugini-Repiquet. On optimal coarse spaces for domain decomposition and their approximation. In *Domain Decomposition Methods in Science and Engineering XXIV 24*, pages 271–280. Springer, 2018.

[28] M. J. Gander and F. Kwok. Optimal interface conditions for an arbitrary decomposition into subdomains. In *Domain Decomposition Methods in Science and Engineering XIX*, pages 101–108. Springer, 2011.

[29] M. J. Gander and A. Loneland. SHEM: An optimal coarse space for RAS and its multiscale approximation. In *Domain Decomposition Methods in Science and Engineering XXIII*, pages 313–321. Springer, 2017.

[30] M. J. Gander, A. Loneland, and T. Rahman. Analysis of a new harmonically enriched multiscale coarse space for domain decomposition methods. *arXiv preprint arXiv:1512.05285*, 2015.

[31] M. J. Gander and B. Song. Complete, optimal and optimized coarse spaces for additive Schwarz. In *Domain Decomposition Methods in Science and Engineering XXIV 24*, pages 301–309. Springer, 2018.

[32] M. J. Gander and T. Vanzan. Heterogeneous optimized Schwarz methods for second order elliptic pdes. *SIAM Journal on Scientific Computing*, 41(4):A2329–A2354, 2019.

[33] M. J. Gander and H. Zhang. A class of iterative solvers for the Helmholtz equation: Factorizations, sweeping preconditioners, source transfer, single layer potentials, polarized traces, and optimized Schwarz methods. *SIAM Review*, 61(1):3–76, 2019.

[34] M. J. Gander and H. Zhang. Schwarz methods by domain truncation. *Acta Numerica*, 31:1–134, 2022.

[35] I. G. Graham, P. O. Lechner, and R. Scheichl. Domain decomposition for multiscale PDEs. *Numer. Math.*, 106(4):589–626, 2007.

[36] A. Heinlein, A. Klawonn, J. Knepper, and O. Rheinbach. Multiscale coarse spaces for overlapping Schwarz methods based on the ACMS space in 2D. *Electronic Transactions on Numerical Analysis*, 48:156–183, 2018.

[37] A. Heinlein, A. Klawonn, J. Knepper, and O. Rheinbach. Adaptive GDSW coarse spaces for overlapping Schwarz methods in three dimensions. *SIAM Journal on Scientific Computing*, 41(5):A3045–A3072, 2019.

[38] A. Heinlein, A. Klawonn, J. Knepper, O. Rheinbach, and O. B. Widlund. Adaptive GDSW coarse spaces of reduced dimension for overlapping Schwarz methods. *SIAM Journal on Scientific Computing*, 44(3):A1176–A1204, 2022.

[39] T. Y. Hou and X.-H. Wu. A multiscale finite element method for elliptic problems in composite materials and porous media. *J. Comput. Phys.*, 134(1):169–189, 1997.

[40] G. Karypis and V. Kumar. A fast and high quality multilevel scheme for partitioning irregular graphs. *SIAM Journal on Scientific Computing*, 20(1):359–392, 1998.

[41] X. S. Li, J. W. Demmel, J. R. Gilbert, L. Grigori, P. Sao, M. Shao, and I. Yamazaki. Superlu users' guide. Technical report, Lawrence Berkeley National Laboratory, 1999.

[42] J. Mandel and M. Brezina. Balancing domain decomposition for problems with large jumps in coefficients. *Math. Comp.*, 65(216):1387–1401, 1996.

[43] J. Mandel and B. Sousedík. Adaptive selection of face coarse degrees of freedom in the BDDC and the FETI-DP iterative substructuring methods. *Computer methods in applied mechanics and engineering*, 196(8):1389–1399, 2007.

[44] L. Marcinkowski and T. Rahman. Additive average Schwarz with adaptive coarse spaces: scalable algorithms for multiscale problems. *ETNA*, 49:28–40, 2018.

[45] F. Nataf and F. Rogier. Factorization of the convection-diffusion operator and the Schwarz algorithm. M^3AS, 5(1):67–93, 1995.

[46] J. M. Nordbotten and P. E. Bjørstad. On the relationship between the multiscale finite-volume method and domain decomposition preconditioners. *Comput. Geosci.*, 12(3):367–376, 2008.

[47] C. Pechstein and R. Scheichl. Analysis of FETI methods for multiscale PDEs. *Numer. Math.*, 111(2):293–333, 2008.

[48] C. Pechstein and R. Scheichl. Analysis of FETI methods for multiscale PDEs. Part II: interface variation. *Numer. Math.*, 118(3):485–529, 2011.

[49] M. Sarkis. Nonstandard coarse spaces and Schwarz methods for elliptic problems with discontinuous coefficients using non-conforming elements. *Numer. Math.*, 77(3):383–406, 1997.

[50] O. Schenk and K. Gärtner. Solving unsymmetric sparse systems of linear equations with PARDISO. *Future Generation Computer Systems*, 20(3):475–487, 2004.

[51] B. Smith, P. Bjorstad, and W. Gropp. *Domain decomposition: parallel multilevel methods for elliptic partial differential equations*. Cambridge University Press, 1996.

[52] N. Spillane, V. Dolean, P. Hauret, F. Nataf, C. Pechstein, and R. Scheichl. Abstract robust coarse spaces for systems of PDEs via generalized eigenproblems in the overlaps. *Numer. Math.*, 126(4):741–770, 2014.

[53] A. Toselli and O. Widlund. *Domain decomposition methods—algorithms and theory*, volume 34 of *Springer Series in Computational Mathematics*. Springer-Verlag, Berlin, 2005.

[54] J. Willems. Spectral coarse spaces in robust two-level Schwarz methods. In *Numerical solution of partial differential equations: theory, algorithms, and their applications*, volume 45 of *Springer Proc. Math. Stat.*, pages 303–326. Springer, New York, 2013.

[55] J. Xu and J. Zou. Some nonoverlapping domain decomposition methods. *SIAM Rev.*, 40(4):857–914, 1998.